Geophysical Research Letters

RESEARCH LETTER
10.1029/2018GL078926

Key Points:
- Both satellite-based observations and climate model simulations of global precipitation are increasingly available at hourly time frequency
- In the observations, most precipitation variance comes from irregular variations within the diurnal cycle
- Models underestimate the overall variance, somewhat underestimating it at daily mean frequency but severely underestimating it at higher frequencies

Supporting Information:
- Supporting Information S1

Correspondence to:
C. Covey,
covey1@llnl.gov

Citation:
Covey, C., Doutriaux, C., Gleckler, P. J., Taylor, K. E., Trenberth, K. E., & Zhang, Y. (2018). High-frequency intermittency in observed and model-simulated precipitation. *Geophysical Research Letters*, *45*. https://doi.org/10.1029/2018GL078926

Received 25 MAY 2018
Accepted 22 AUG 2018
Accepted article online 29 AUG 2018

High-Frequency Intermittency in Observed and Model-Simulated Precipitation

Curt Covey[1], Charles Doutriaux[1], Peter J. Gleckler[1], Karl E. Taylor[1], Kevin E. Trenberth[2], and Yongxin Zhang[2]

[1]Program for Climate Model Diagnosis and Intercomparison, Lawrence Livermore National Laboratory, Livermore, CA, USA, [2]Climate Analysis Section/Climate and Global Dynamics Laboratory, National Center for Atmospheric Research, Boulder, CO, USA

Abstract A newly reprocessed, bias-corrected version of hourly satellite observations that provides global coverage of precipitation at high space-time resolution is evaluated and compared with climate model simulations. Irregular subdaily fluctuations are the dominant component around the world, greater than variance of daily mean precipitation, and much greater than variance associated with the mean diurnal cycle of precipitation. Irregular subdaily fluctuations of precipitation are severely underestimated by models, even after taking into account the observational "error bars" implied by different space-time resolutions. Variance of daily mean precipitation is less severely underestimated. Although mean diurnal cycle amplitudes vary among the models, this component is but a small part of total precipitation variance. Therefore, the total precipitation variance is significantly underestimated by models in general. Further exploration of model-data discrepancies in precipitation at high-time frequency may lead to new and useful climate model diagnostics.

Plain Language Summary Satellite-estimated rainfall rates at high spatial resolution and high-time frequency can be compared with output from modern climate models. Here we examine the statistical variability of observed and model-simulated rainfall. Total variability divides naturally into three separate components, arising from (a) intermittent rainfall fluctuations at time scales less than a day, (b) variations of daily totals of rainfall, and (c) the average day-to-night cycle of rainfall. Observations show that in reality the first component dominates the total. Climate models, however, systematically underestimate the first component (though their errors in the other two are not as severe). Diagnosing the sources of these errors may provide a new way to improve climate model accuracy.

1. Introduction

High-frequency precipitation records include not only a mean diurnal cycle and longer time scale statistics, such as daily and monthly means, but also an "intermittency" component associated with the original high-frequency values (Trenberth et al., 2017). The overwhelming fraction of precipitation variance comes from day-to-day variations at each hour of the diurnal cycle. This disproportionality is consistent with the observation that even in tropical convergence zones, it rains far less than half the time (Trenberth & Zhang, 2018a). The extent of disproportionality can be inferred from Figure 4 of a recent paper in which $\pm 1\sigma_{SE}$ error bars on observations of the diurnal cycle were shown (Covey et al., 2016; σ_{SE} is the standard error of the mean, that is, the standard deviation of hourly values normalized by the square root of the number of days N). Values of σ_{SE} in the figure are generally less than the amplitude of the diurnal cycle, but the standard deviation of hourly values $\sqrt{N}\sigma_{SE}$ is always much greater. Hence, the variance associated with the subdaily fluctuations is greater than that of the daily means, which in turn is much greater than that of the mean diurnal cycle.

The present study elucidates this point and compares observations with a diverse set of climate model simulations. We find that high-frequency variance of precipitation is seriously underestimated by the simulations.

2. Data Sources

We compare two recent satellite-based data sets of precipitation—Tropical Rainfall Measuring Mission (TRMM) version 3B42 (Huffman et al., 2007) and bias-corrected CMORPH v1.0 CRT (Xie et al., 2017)—with the most recent high-time resolution output from the Community Earth System Model (CESM1) and with

a somewhat less recent multimodel ensemble gathered by the Coupled Model Intercomparison Project Phase 5 (CMIP5; Taylor et al., 2012). We use CESM1 output from an ensemble of 30 coupled ocean-atmosphere-sea-ice model runs with varying initial conditions (Kay et al., 2015). Results from the two ensemble members that recorded output at hourly time frequency (#34 and #35) are shown below.

Both TRMM 3B42 and bias-corrected CMORPH use ground-based precipitation measurements to calibrate the satellite data. Two different methods are used to infill sparse microwave observations: TRMM 3B42 depends on outgoing longwave radiation, which is correlated with clouds and precipitation; CMORPH employs cloud-tracked winds to advect rainy areas. As both methods have their own strengths and weaknesses (Tian et al., 2007) comparing them with each other illustrates one aspect of observational uncertainty. In addition, CMORPH data (and the CESM1 output studied here) are recorded at hourly frequency whereas TRMM data (and CMIP5 output) are at 3-hourly frequency, allowing us to test the sensitivity of results to frequency. Finally, since the satellite-based data sets are at higher spatial resolution (0.25° latitude/longitude) than most climate models, we regrid both CMORPH and TRMM data to match the resolution of the CESM1 (~1° latitude/longitude) in some of the results presented below, in order to test resolution sensitivity.

All data sets discussed in this paper are in the public domain; data processing used the open-source Community Data Analysis Tools (https://uvcdat.llnl.gov). TRMM data are at disc.gsfc.nasa.gov/datasets/TRMM_3B42_V7/summary?keywords=TRMM_3B42 and http://mirador.gsfc.nasa.gov. CMORPH data (http://www.cpc.ncep.noaa.gov/products/janowiak/cmorph_description.html; ftp://ftp.cpc.ncep.noaa.gov/precip/CMORPH_V1.0/REF/EGU_1104_Xie_bias-CMORPH.pdf) are downloadable at ftp://ftp.cpc.ncep.noaa.gov/precip/global_CMORPH/30min_8km. CESM-LE output is available via the Earth System Grid: https://www.earthsystemgrid.org. CMIP5 output is available at https://cmip.llnl.gov/cmip5/data_getting_started.html.

3. Analysis Methods

Starting from hourly or 3-hourly precipitation data, we resolve the time series into components isolating variations associated with monthly, daily, and subdaily time scales. For each month, let $X_{i,n}$ be a time-point value for hour i of day n with $n = 1, 2, \ldots, N$ days and $i = 1, 2, \ldots, D$. ($D = 24$ for hourly data, $D = 8$ for 3-hourly data, etc.) The relevant means are

1. the mean diurnal cycle $\overline{X_i^{\mathrm{dc}}} \equiv N^{-1}\Sigma_{n=1}^{N} X_{i,n}, \quad i = 1, 2, \ldots, D$
2. the daily mean $\overline{X_n^{\mathrm{dm}}} \equiv D^{-1}\Sigma_{i=1}^{D} X_{i,n}, \quad n = 1, 2, \ldots, N$
3. the overall monthly mean $\overline{X^{\mathrm{all}}} \equiv N^{-1}\Sigma_{n=1}^{N}\overline{X_n^{\mathrm{dm}}} = D^{-1}\Sigma_{i=1}^{D}\overline{X_i^{\mathrm{dc}}}$

Note that $\overline{X_i^{\mathrm{dc}}}$ includes all Fourier harmonics in the daily cycle (once a day "diurnal" term, twice a day "semidiurnal" term, thrice a day "terdiurnal" term, . . .), but it does not include subdaily periods that are not simple harmonics of 24 hr, for example, the principal lunar semidiurnal period of 12.4 hr.

The corresponding variances are

1. $\sigma_{\mathrm{mdc}}^2 \equiv D^{-1}\Sigma_{i=1}^{D}\left(\overline{X_i^{\mathrm{dc}}} - \overline{X^{\mathrm{all}}}\right)^2$
2. $\sigma_{\mathrm{dm}}^2 \equiv N^{-1}\Sigma_{n=1}^{N}\left(\overline{X_n^{\mathrm{dm}}} - \overline{X^{\mathrm{all}}}\right)^2$
3. $\sigma_{\mathrm{all}}^2 \equiv (D\,N)^{-1}\Sigma_{i,n}\left(X_{i,n} - \overline{X^{\mathrm{all}}}\right)^2$

We resolve the overall variance σ_{all}^2 into three orthogonal components: variance of the mean diurnal cycle σ_{mdc}^2, variance of daily means σ_{dm}^2, and a final term that arises from irregular subdaily variations, $\sigma_{\mathrm{isd}}^2 \equiv \sigma_{\mathrm{all}}^2 - \sigma_{\mathrm{mdc}}^2 - \sigma_{\mathrm{dm}}^2$. Thus,

$$\sigma_{\mathrm{all}}^2 = \sigma_{\mathrm{dm}}^2 + \sigma_{\mathrm{mdc}}^2 + \sigma_{\mathrm{isd}}^2 \tag{1}$$

by definition. Equation (1) may also be derived by first resolving $X_{i,n}$ into components associated with the mean diurnal cycle, the daily means, and a third "remainder" term and then conducting the usual analysis of variance (Fisher, 1919; Taylor & Covey, 2018).

The standard deviation of daily means σ_{dm} is a traditional measure of high-frequency climate variability, but it will be less than the total σ_{all} if there are any subdaily variations. How much less? One indication comes from another quantity: the day-to-day variance of hourly values $\sigma_h^2 \equiv N^{-1}\sum_{n=1}^{N}\left(X_{i,n} - \overline{X_i^{dc}}\right)^2$, which was discussed in section 1. Note that σ_h^2 is a function of time-of-day i. Straightforward algebra (Covey & Gehne, 2016) demonstrates that

$$\sigma_{dm}^2 + \sigma_{isd}^2 = D^{-1}\sum_{i=1}^{D}\sigma_h^2. \quad (2)$$

Previous work shows that if $\overline{X_i^{dc}}$ and $\overline{X_j^{dc}}$ are uncorrelated for $i \neq j$, then $\sigma_{dm}^2 = D^{-2}\sum_{i=1}^{D}\sigma_h^2$ (Trenberth et al., 2017). In this case the variance of daily means is reduced by an extra factor D from the average variance of hourly values. Observational results presented below show that $\sigma_{isd} > \sigma_{dm} \gg \sigma_{mdc}$ on the right-hand side of (1). Therefore, σ_{dm} should be reduced from σ_{all} by a factor somewhat less than $\sqrt{D}$, depending on correlations between $\overline{X_i^{dc}}$ and $\overline{X_j^{dc}}$.

4. Results

Figures 1 and 2 show statistics from observational data sets and from model simulations, respectively, for composite Julys spanning 1998–2013. (Composite Januarys give similar results, as shown in Table 1 and Figures S1–S2 in the supporting information.) Each figure shows standard deviations of irregular subdaily variations, of daily means, and of the mean diurnal cycle (σ_{isd}, σ_{dm}, and σ_{mdc}, respectively). The standard deviations are shown as maps for CMORPH observations in Figure 1 and for one member of the CESM large ensemble in Figure 2. Zonal means appear to the right of the corresponding maps, with additional data sources included. The latitude coverage in all graphics is restricted to the TRMM 3B42 range 50°S–50°N for an apples-to-apples comparison of all data sets.

The same color scale is used for maps in Figures 1 and 2 in order to directly compare the model with observations. To bring out relevant details, zonal means for the three fields are presented at different scales: maxima for σ_{isd}, σ_{dm}, and σ_{mdc} are 30, 20, and 4 mm/day respectively. In zonal mean plots of Figure 2, selected observations from Figure 1 appear for comparison.

Inspection reveals that $\sigma_{isd} > \sigma_{dm} \gg \sigma_{mdc}$ in the observed data (Figure 1), as claimed above. Latitude/longitude patterns of σ_{isd} and σ_{dm} are virtually identical; only minor differences in pattern can be seen, for example, comparing CMORPH July zonal mean σ_{isd} and σ_{dm} around 20°N. All three standard deviations follow the pattern of observed monthly mean precipitation (*not shown*) with more average rainfall implying more variance of rainfall. Given that precipitation is positive definite, this is not surprising, but the ratio of the two dominant components σ_{isd} and σ_{dm} is remarkably uniform with latitude and across data sets (supporting information Figures S3–S4).

Comparing Figures 1 and 2 shows that the model underestimates σ_{isd} by roughly a factor of 2–3 at most latitudes, σ_{dm} by a factor of 2 at most latitudes, and σ_{mdc} by a factor of 2 in the tropics. As with the observations, the model's latitude/longitude patterns of standard deviation closely follow the simulated monthly mean precipitation. For example, a problematic "Doubled Intertropical Convergence Zone" is evident in the Pacific (Figure 2c).

From equation (1), together with the CESM1's factor of 2 underestimate of σ_{isd} and σ_{dm}, it follows that the model misses around three fourths of the total high-frequency variance σ_{all}^2. (The underestimate of σ_{mdc} contributes little to the total error since its relative contribution to σ_{all} is small.) This result suggests that comparisons of model versus observed precipitation variance are incomplete if they do not include subdaily frequencies.

Zonal means of both Members #34 and #35 of the CESM large ensemble are shown in Figure 2. The nearly identical curves imply that 16-year compilations are sufficient to remove chaotic fluctuations from high-frequency intermittency statistics, so a single ensemble member proves adequate to characterize the performance of the model.

Precipitation variance can be sensitive to space and time resolution of the data (Rind et al., 1989). To explore this issue, zonal mean panels of Figure 1 show CMORPH and TRMM data both at their original 0.25° resolution

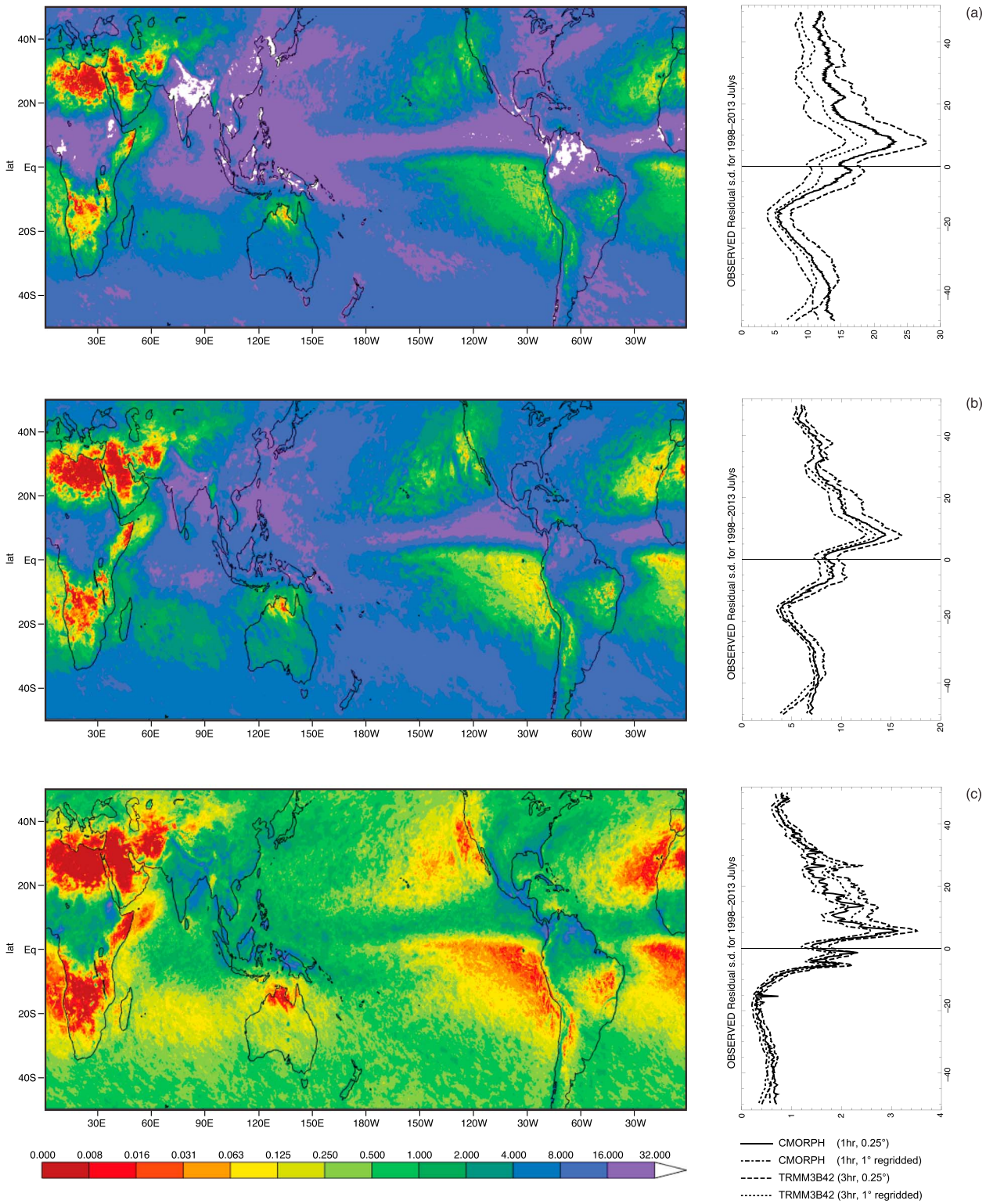

Figure 1. Observed standard deviations of three orthogonal components of precipitation variance: (a) "residual" standard deviation associated with irregular sub-daily variations, (b) standard deviation of daily means, and (c) standard deviation of the mean diurnal cycle. Left-hand panels map bias-corrected CMORPH hourly data (0.25° latitude/longitude resolution) for composite Julys of the years 1998–2013. Right-hand panels show zonal means (root-mean-square) of CMORPH and TRMM data at their original resolution (0.25° latitude/longitude) and regridded to match the coarser resolution of the CESM1 model (~1° latitude/longitude). TRMM = Tropical Rainfall Measuring Mission; s.d. = standard deviation.

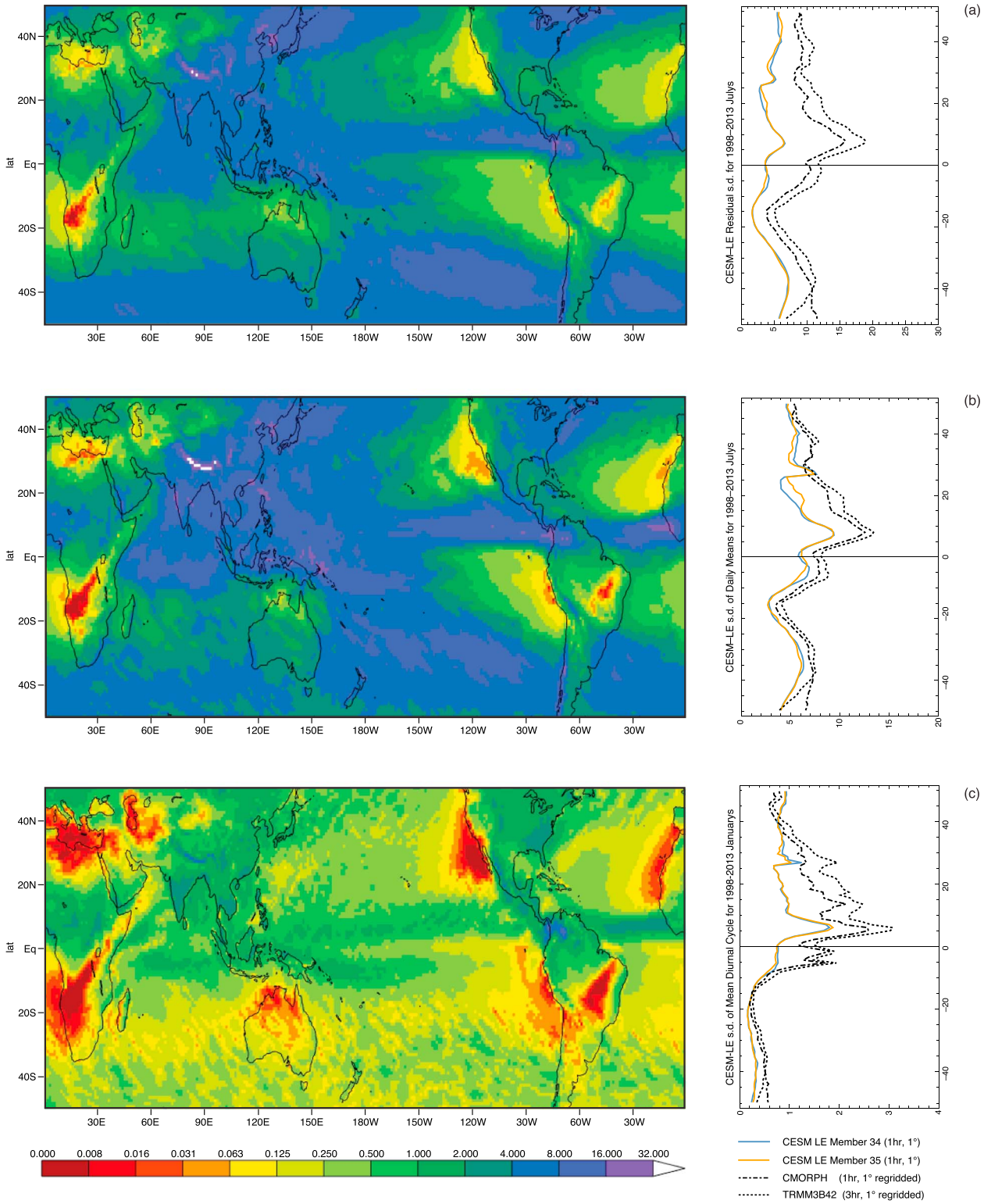

Figure 2. Same standard deviations as in Figure 1 for CESM1 large ensemble simulations (for the same time periods: Composite Julys of the years 1998–2013). Left-hand panels map output from ensemble Member #35 (the same member examined in Trenberth et al., 2017). Right-hand panels show zonal means (root-mean-square) of the Member #35 output together with corresponding zonal means from Member #34. Also shown in the zonal mean plots, for comparison with observations, are data from the subset of Figure 1 in which CMORPH and TRMM are regridded to match the coarser resolution of CESM1. TRMM = Tropical Rainfall Measuring Mission; CESM1 = Community Earth System Model version 1; CESM LE = Community Earth System Model large ensemble; s.d. = standard deviation.

Table 1
Orthogonal Components of Variance, Averaged Over Ocean and Land Areas (Standard Deviations in Millimeters per Day)

	Land σ_{ISD}	Ocean σ_{ISD}	Land σ_{DM}	Ocean σ_{DM}	Land σ_{MDC}	Ocean σ_{MDC}
January CMORPH (0.25°)	13.81	13.25	7.41	9.36	1.78	0.93
January CMORPH (1.00°)	10.45	13.06	5.98	8.54	1.55	0.79
January TRMM3B (0.25°)	16.02	15.52	8.12	9.77	2.21	1.09
January TRMM3B (1.00°)	12.41	14.10	6.58	8.59	2.00	0.92
January CESM#34 (1.00°)	3.94	5.30	4.99	6.36	1.12	0.53
January CESM#35 (1.00°)	3.90	5.19	4.91	6.18	1.14	0.53
July CMORPH (0.25°)	15.13	12.89	7.41	8.68	1.99	1.00
July CMORPH (1.00°)	11.15	12.33	6.03	7.90	1.70	0.88
July TRMM3B (0.25°)	17.08	15.57	8.42	9.64	2.38	1.23
July TRMM3B (1.00°)	12.93	13.93	6.69	8.42	2.10	1.08
July CESM#34 (1.00°)	4.49	4.88	5.28	5.83	1.12	0.59
July CESM #35 (1.00°)	4.50	4.84	5.22	5.87	1.12	0.58

Note. Observed global means are shown in Figure 3. ISD = s.d. of intermittent subdiurnal variations; DM = s.d. of daily means; MDC = s.d. of mean diurnal cycle; CESM = Community Earth System Model; TRMM = Tropical Rainfall Measuring Mission; s.d. = standard deviation.

and regridded to the CESM1's 1° resolution. Comparing results within each panel suggests that observed σ_{dm} and σ_{mdc} are not very sensitive to space or time resolution; σ_{isd} however increases by a noticeable amount when hourly CMORPH data are replaced by 3-hourly TRMM at the same 0.25° resolution, and it decreases for both CMORPH and TRMM when resolution is degraded to 1°.

To better quantify the foregoing results, Table 1 gives spatial averages of the statistics in Figures 1, 2, taken separately over all land areas and all ocean areas, including January as well as July. Land averages and ocean averages are similar for both σ_{isd} and σ_{dm}, in both the observations and the CESM1 simulations. But σ_{mdc} is a factor of ~2 larger over land than over ocean (as expected from the spatially averaged Fourier amplitudes shown in Covey et al., 2016). Also, July values are about equal to their corresponding January values (to within ~10%) when averaged over these large scales.

Regarding the effect of space and time resolution of the data, Table 1 confirms that observed values of the standard deviations are moderately sensitive to changing the data source from hourly CMORPH to 3-hourly TRMM. Coarsening the grid decreases all components of variance, as expected (Trenberth et al., 2017). The observational standard deviations change by less than 25%—and usually much less—as the data source is varied. But CESM1-simulated standard deviations are a great deal less than observed. Compared with CMORPH, the model-simulated values of σ_{isd} are lower by more than a factor of 2. For σ_{dm}, the model's simulated values are roughly four fifths of the observed values, a smaller but probably still a significant underestimate. The CESM1 also underestimates σ_{mdc} by up to a factor of 2.

Do these problems generalize from CESM1 to other climate models? To address this question, Figure 3 shows high-time-frequency statistics from the CMIP5 multimodel ensemble. This is the most recent version of CMIP. It predates development of the CESM1, though it includes its immediate predecessor, the Community Climate System Model version 4. Global spatial averages of σ_{isd}, σ_{dm}, and σ_{mdc} from the CMIP5 models are shown as histograms in Figure 3; corresponding observed values appear as vertical lines. Individual models are identified in supporting information (Table S1).

Figure 3 indicates that the CESM1's underpredictions of σ_{isd} and σ_{dm} generalize to the climate models that provided high-time-frequency output to CMIP5. Nearly all versions of the observed σ_{isd} values lie to one side of nearly all model-simulated values. The only exception is one model with a global mean value of σ_{isd} in between the coarsened 1° versions of CMORPH and TRMM—but this model has 0.56° resolution (Sakamoto et al., 2012) and thus should be assessed against observations falling between the 1° and original 0.25° observations of CMORPH and TRMM, not the plotted 1° lines.

In light of observational uncertainty, conclusions from Figure 3 must be made cautiously. Nevertheless, the sizeable gap between all but one model and all four versions of the observations (as well as the gap between CESM1 and observations shown in the zonal means of Figure 2) implies that climate models severely underestimate variance of precipitation at subdaily frequencies. Separately, values of σ_{dm} are greater than most

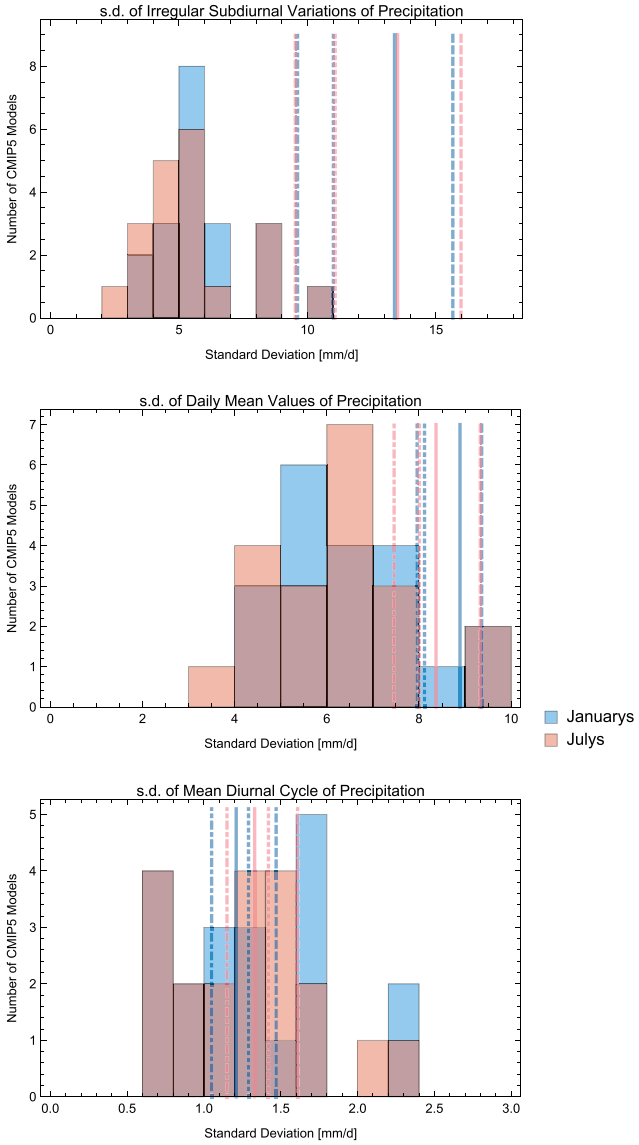

Figure 3. Histograms of global averages (root-mean-square) of the three standard deviations in Figures 1–2: (top) "residual" standard deviation associated with irregular subdaily variations, (middle) standard deviation of daily means, and (bottom) standard deviation of the mean diurnal cycle. Global averages of the observations in Figure 1 are added as vertical lines, coded as in Figure 1. Both composite Januarys (blue) and composite Julys (orange) of the years 1998–2013 are shown; brown color indicates where the histograms overlap. CMIP5 = Coupled Model Intercomparison Project Phase 5; s. d. = standard deviation.

(but not all) model-simulated values in Figure 3, suggesting that models in general underestimate the variance of daily means. In contrast, observed values of σ_{mdc} are near the median of model-simulated values; the CESM1's underprediction of this component is not a feature of climate models in general.

5. Discussion

Data at subdaily time frequency can reveal the connection between weather and climate. One example is derivation of the mean diurnal cycle of rainfall from individual storms, as shown in Figure S11 of Covey et al. (2016). Higher-order statistics of precipitation, however, are relatively unexplored at time scales shorter than daily means. Yet intermittency on such time scales affects human and natural ecosystems through precipitation extremes (Gehne et al., 2016; Kendon et al., 2017; Prein et al., 2015), and the CMIP5 models predict that under global warming scenarios, the standard deviation of precipitation will increase by an amount that is "remarkably robust on a range of time scales" from decadal down to at least daily (Pendergrass et al., 2017). This prediction is consistent with a longstanding suggestion that in a warmer world, "individual storms could be more intense from the latent heat enhancement, but fewer and farther between" (Trenberth, 1998).

Apart from any effect on predicted climate impacts, errors in high-time-frequency statistics of precipitation would raise the possibility of erroneous processes that generate clouds and precipitation in a model. The present work shows that at hourly and 3-hourly time frequencies, the main component of precipitation variance around the world is irregular fluctuations within the diurnal cycle. Climate models seriously underestimate the magnitude of this component. Variance of daily mean precipitation, a more familiar part of climate model diagnosis, is somewhat better simulated by the models. The mean diurnal cycle contributes a third component, but it is just a small fraction of the total. Figures 2 and 3 show that dependence on grid resolution (and the difference between choosing CMORPH versus TRMM observations) is swamped by the difference between observations and model simulations. This result implies that the discrepancy between models and observations is robust to considerations of observational uncertainty.

The present study follows previous work that used the same data from CMORPH, TRMM, and CESM1 but focused on the duration of precipitation events and found that the model "precipitates far too often at low rates and not enough for intense rates" (Trenberth et al., 2017). Earlier comparisons of models with ground-based (Sun et al., 2006) and CloudSat (Stephens et al., 2010) observations reached similar conclusions; the latter study found that even a model whose resolution permits explicitly simulated convection underestimated the intensity of precipitation at midlatitudes by a factor of 2–3 (Stephens et al., 2010, Figure 8c). Although the present study's findings are consistent with previous work, our analysis method does not directly involve duration of precipitation events; hence, it cannot infer a spectrum of precipitation intensity versus frequency. But σ_{isd} and the other terms in equation (1) provide quantitative metrics of model performance that are especially useful for intercomparing a large number of different data sets, as in Figure 3.

Of course, more work is needed to better understand observational uncertainty of precipitation and its implications for model evaluation, particularly at subdaily time scales. Dependence of variance on space-time resolution is one source of this uncertainty. An additional problem is that satellites give nearly

instantaneous precipitation rates, whereas model output is typically accumulated over time (e.g., 3-hr intervals for CMIP5 data). This problem may be reduced by comparing model output from individual time steps (as in Stephens et al., 2010) with very high-frequency observations, such as half-hourly data from the Global Precipitation Mission launched in 2014. The current version of this data is useful for assessing particular events, for example, Hurricane Harvey (Trenberth et al., 2018), although its 4-year time coverage is too short for the present analysis. Despite these uncertainties, it is worth noting that all data sets discussed in this paper incorporate extensive ground-based precipitation data in calibrating the satellite observations, and that direct comparison of 3-hourly weather reports with satellite-based data gives comparable subdaily frequencies of precipitation (Dai et al., 2007).

The results presented in this paper imply that traditional diagnostics at daily and longer time scales can miss a great deal of the discrepancy between models and observations of precipitation. A similar inference may follow from covariability of the hourly CMORPH data, which "demonstrate [s] that daily averages fail to capture the essential character of precipitation" (Trenberth & Zhang, 2018b). Thus, high-time-frequency statistics of precipitation and of other fields such as cloudiness, surface temperature, and pressure (Covey et al., 2014; Lewis & Karoly, 2013; Lindvall & Svensson, 2015; Zhang & Klein, 2013) can lead to new and useful climate model diagnostics, aiding insight into atmospheric processes.

Acknowledgments
This research was conducted at the National Center for Atmospheric research, which is sponsored by the U.S. National Science Foundation, and under auspices of Regional and Global Climate Model Analysis, Office of Science, U.S. Department of Energy at the Lawrence Livermore National Laboratory under contract DE-AC52-07NA27344 (grant DE-SC0012711). All data sets used in this analysis are publicly available as described in section 2.

References

Covey, C. D., Lindzen, R. S., & Marsh, D. (2014). Atmospheric tides in the latest generation of climate models. *Journal of the Atmospheric Sciences*, *71*(6), 1905–1913. https://doi.org/10.1175/JAS-D-13-0358.1

Covey, C., & Gehne, M. (2016). Variance of high-frequency precipitation. LLNL Technical Report #694199. Retrieved from https://e-reports-ext.llnl.gov/pdf/823104.pdf

Covey, C., Gleckler, P. J., Doutriaux, C., Williams, D. N., Dai, A., Fasullo, J., et al. (2016). Metrics for the diurnal cycle of precipitation: Toward routine benchmarks for climate models. *Journal of Climate*, *29*(12), 4461–4471. https://doi.org/10.1175/JCLI-D-15-0664.1

Dai, A., Lin, X., & Hsu, K.-L. (2007). The frequency, intensity, and diurnal cycle of precipitation in surface and satellite observations over low- and mid-latitudes. *Climate Dynamics*, *29*(7-8), 727–744. https://doi.org/10.1007/s00382-007-0260-y

Fisher, R. A. (1919). The correlation between relatives on the supposition of Mendelian inheritance. *Philosophical Transactions of the Royal Society of Edinburgh*, *52*(02), 399–433. https://doi.org/10.1017/S0080456800012163

Gehne, M., Hamill, T. M., Kiladis, G. N., & Trenberth, K. E. (2016). Comparison of global precipitation estimates across a range of temporal and spatial scales. *Journal of Climate*, *29*(21), 7773–7795. https://doi.org/10.1175/JCLI-D-15-0618.1

Huffman, G. J., Adler, R. F., Bolvin, D. T., Gu, G. J., Nelkin, E. J., Bowman, K. P., et al. (2007). The TRMM multisatellite precipitation analysis (TMPA): Quasi-global, multiyear, combined-sensor precipitation estimates at fine scales. *Journal of Hydrometeorology*, *8*(1), 38–55. https://doi.org/10.1175/JHM560.1

Kay, J. E., Deser, C., Phillips, A., Mai, A., Hannay, C., Strand, G., et al. (2015). The Community Earth System Model (CESM) large ensemble project: A community resource for studying climate change in the presence of internal climate variability. *Bulletin of the American Meteorological Society*, *96*(8), 1333–1349. https://doi.org/10.1175/BAMS-D-13-00255.1

Kendon, E., Ban, N., Roberts, N. M., Fowler, H. J., Roberts, M. J., Chan, S. C., et al. (2017). Do convection-permitting regional climate models improve projections of future precipitation change. *Bulletin of the American Meteorological Society*, *98*(1), 79–93. https://doi.org/10.1175/BAMS-D-15-0004.1

Lewis, S. C., & Karoly, D. J. (2013). Evaluation of historical diurnal temperature range trends in CMIP5 models. *Journal of Climate*, *26*(22), 9077–9089. https://doi.org/10.1175/JCLI-D-13-00032.1

Lindvall, J., & Svensson, G. (2015). Diurnal temperature range in the CMIP5 models. *Climate Dynamics*, *44*(1-2), 405–421. https://doi.org/10.1007/s00382-014-2144-2

Pendergrass, A. G., Knutti, R., Lehner, F., Deser, C., & Sanderson, B. M. (2017). Precipitation variability increases in a warmer climate. *Scientific Reports*, *7*(1), 17966. https://doi.org/10.1038/s41598-017-17966-y

Prein, A. F., Langhans, W., Fosser, G., Ferrone, A., Ban, N., Goergen, K., et al. (2015). A review on regional convection-permitting climate modeling: Demonstrations, prospects and challenges. *Reviews of Geophysics*, *53*, 323–361. https://doi.org/10.1002/2014RG000475

Rind, D., Goldberg, R., & Ruedy, R. (1989). Change in climate variability in the 21st century. *Climatic Change*, *14*(1), 5–37. https://doi.org/10.1007/BF00140173

Sakamoto, T. T., Komuro, Y., Nishimura, T., Ishii, M., Tatebe, H., Shiogama, H., et al. (2012). MIROC4h—A new high-resolution atmosphere-ocean coupled general circulation model. *Journal of the Meteorological Society of Japan*, *90*(3), 325–359. https://doi.org/10.2151/jmsj.2012-301

Stephens, G. L., L'Ecuyer, T., Forbes, R., Gettelmen, A., Golaz, J.-C., Bodas-Salcedo, A., et al. (2010). Dreary state of precipitation in global models. *Journal of Geophysical Research*, *115*, D24211. https://doi.org/10.1029/2010JD014532

Sun, Y., Solomon, S., Dai, A., & Portmann, R. W. (2006). How often does it rain? *Journal of Climate*, *19*(6), 916–934. https://doi.org/10.1175/JCLI3672.1

Taylor, K. E., & Covey, C. (2018). Analysis of variance including the diurnal cycle. LLNL Technical Report #753967. Retrieved from https://www.osti.gov/servlets/purl/1460516

Taylor, K. E., Stouffer, R. J., & Meehl, G. A. (2012). An overview of CMIP5 and the experiment design. *Bulletin of the American Meteorological Society*, *93*(4), 485–498. https://doi.org/10.1175/BAMS-D-11-00094.1

Tian, Y., Peters-Lidard, C. D., Choudhury, B. J., & Garcia, M. (2007). Multitemporal analysis of TRMM-based satellite precipitation products for land data assimilation applications. *Journal of Hydrometeorology*, *8*, 1166–1183.

Trenberth, K. E. (1998). Atmospheric moisture residence times and cycling: Implications for rainfall rates and climate change. *Climatic Change*, *39*(4), 667–694. https://doi.org/10.1023/A:1005319109110

Trenberth, K. E., Cheng, L., Jacobs, P., Zhang, X., & Fasullo, J. (2018). Hurricane Harvey links to ocean heat content and climate change adaptation. *Earth's Future*, *6*(5), 730–744. https://doi.org/10.1029/2018EF000825

Trenberth, K. E., & Zhang, Y. (2018a). How often does it really rain? *Bulletin of the American Meteorological Society*, *99*(2), 289–298. https://doi.org/10.1175/BAMS-D-17-0107.1

Trenberth, K. E., & Zhang, Y. (2018b). Near-global covariability of hourly precipitation in space and time. *Journal of Hydrometeorology*, *19*(4), 695–713. https://doi.org/10.1175/JHM-D-17-0238.1

Trenberth, K. E., Zhang, Y., & Gehne, M. (2017). Intermittency in precipitation: Duration, frequency, intensity, and amounts using hourly data. *Journal of Hydrometeorology*, *18*(5), 1393–1412. https://doi.org/10.1175/JHM-D-16-0263.1

Xie, P. R., Joyce, S. W., Yoo, S.-H., Yaroah, Y., Sun, F., & Lin, R. (2017). Reprocessed, bias-corrected CMORPH global high-resolution precipitation estimates from 1998. *Journal of Hydrometeorology*, *18*(6), 1617–1641. https://doi.org/10.1175/JHM-D-16-0168.1

Zhang, Y., & Klein, S. A. (2013). Factors controlling the vertical extent of fair-weather shallow cumulus clouds over land: Investigation of diurnal-cycle observations collected at the ARM Southern Great Plains site. *Journal of the Atmospheric Sciences*, *70*(4), 1297–1315. https://doi.org/10.1175/JAS-D-12-0131.1